Available online at www.sciencedirect.com
ScienceDirect
Bioelectrochemistry 69 (2006) 25 – 33
Bioelectrochemistry
www.elsevier.com/locate/bioelechem

Remote NADH imaging through an ordered array of electrochemiluminescent nanoapertures

Arnaud Chovin, Patrick Garrigue, Neso Sojic *

Laboratoire d'Analyse Chimique par Reconnaissance Moléculaire, Université Bordeaux I, ENSCPB, 16 avenue Pey-Berland, 33607 Pessac, France

Received 29 July 2005; received in revised form 7 October 2005; accepted 14 October 2005
Available online 13 December 2005

Abstract

In this report, we present an ordered array comprising thousands of nanoapertures for the electrochemiluminescent (ECL) detection of NADH. It was fabricated on the distal face of a coherent optical fiber bundle. Such a high-density array of nanoapertures combines optical, imaging and electrochemical properties. Indeed, each nanoaperture is surrounded by a gold nanoring, which acts as an electrode material. The behavior of the array was characterized by cyclic voltammetry and it shows excellent electrochemical performances. NADH is the analyte, which is measured in presence of $Ru(bpy)_3^{2+}$. The ruthenium complex mediates the NADH oxidation and this coenzyme acts as a co-reactant in the ECL mechanism. ECL light is generated at the distal face of the array by each gold ring electrode. A fraction of this ECL light is collected by the corresponding nanoaperture, transmitted through the optical fiber bundle and finally imaged on the proximal face with a CCD camera. In this work, we show that NADH concentration is remotely detected by an oxidative-reductive ECL mechanism. We present also some preliminary results about the ECL process of NADH with $Ru(bpy)_3^{2+}$. The ECL behavior of NADH on gold surface is reported. The influence of the applied potential on the collected light intensity was investigated. The variation of the ECL intensity measured through the nanoaperture array with NADH concentration is linear. Remote ECL detection of NADH is spatially resolved over a large area with a micrometer resolution through the array. Therefore, such array integrates several complementary functions: ECL light generation, collection, transmission and remote imaging in an array format.

Keywords: Electrochemiluminescence; NADH; Array; Nanoaperture; Optical fiber bundle

1. Introduction

The nicotinamide coenzyme (NAD^+/NADH) controls the enzymatic activity of more than 300 dehydrogenases. NADH acts as a source of two electrons and a proton, which is equivalent to a hydride ion. This class of enzymes catalyzes the oxidation of a large variety of clinically important analytes, such as alcohols, aldehydes and carbohydrates. Dehydrogenases are widely used in bioanalytical chemistry, mainly in enzymatic assays. Another potential field of commercial applications is the enzymatic electrodes [1,2]. However, the performances of the dehydrogenase-based biosensors are limited by the electrochemical detection or the regeneration of the active form of the coenzyme. Indeed, oxidation of NADH requires a high overpotential at most of the bare-electrode surfaces. Moreover, the products of NADH oxidation adsorb strongly and passivate the electrode surface. This process is accelerated when NAD^+ is present. Among the different strategies to overcome these issues, a highly studied way is the use of redox mediators. The large overpotential associated to NADH oxidation is then highly reduced. By monitoring the electrocatalytic current corresponding to the regeneration of the coenzyme via the redox mediator, the enzymatic activity is directly measured and thus the concentration of the enzymatic substrate. However, the selectivity remains an issue since others easily oxidized interferents can also be detected. An attractive alternative is the re-oxidation of this coenzyme by an ECL species, such as ruthenium(II) tris(2,2′-bipyridine) [3–5]. This $Ru(bpy)_3^{2+}$ mediates the NADH oxidation and an excited state can be generated by this process. NADH acts therefore as a co-reactant in the ECL

* Corresponding author. Tel.: +33 5 4000 2496; fax: +33 5 4000 2717.
E-mail address: sojic@enscpb.fr (N. Sojic).

1567-5394/$ - see front matter © 2005 Elsevier B.V. All rights reserved.
doi:10.1016/j.bioelechem.2005.10.002

mechanism. The reduced form, NADH, initiates ECL reaction in presence of the ruthenium complex whereas the oxidized form of the coenzyme, NAD^+, does not. Indeed, it has been reported that aromatic amines, such as the pyridine ring of NAD^+, do not generate chemiluminescence with $Ru(bpy)_3^{3+}$ [6]. In NADH, the aromaticity of the pyridine ring is destroyed and the aliphatic tertiary amine group undergoes ECL emission [6]. Thus, ECL light could then be electrocatalytically generated in presence of the enzyme and of the substrate [6–9]. The substrate concentration is monitored just by measuring the ECL intensity, which is directly related to the variations of the NADH concentration. It means that the analytical signal is then not the faradaic current but the resulting ECL intensity. Hence, using this ECL scheme, many species that are of great interest in bioanalysis can be detected by coupling them to dehydrogenase enzymes that convert NAD^+ to NADH.

ECL is the electrogenerated emission of light from an electronically excited state which is produced by energetic electron transfer reaction. The ECL process is initiated by an electron transfer occurring directly at the electrode surface [10,11]. The earliest ECL reactions were carried out in aprotic solvents and occurred by the annihilation reaction. For bioanalytical applications, ECL emission in aqueous solution is based on a mechanism involving a co-reactive species. The co-reactant can be treated therefore as an analyte. This development has opened up a great variety of new applications in analytical chemistry and medical diagnostics [12]. ECL has been widely applied in this configuration to detect various analytes, such as hydrogen peroxide, oxalate, chlorpromazine, antibiotics and proteins with secondary amine groups [13–15]. The co-reactant produces a highly oxidizing or highly reducing species in a reaction following a homogeneous or heterogeneous electron transfer reaction. This approach is very useful since ECL emission occurs in water after applying a simple potential step. The excited state of the ECL emitter is formed either by an oxidative-reduction mechanism or reductive-oxidation mechanism. A commonly used system for co-reactant ECL involves the ruthenium complex, $Ru(bpy)_3^{2+}$. ECL mechanism of $Ru(bpy)_3^{2+}$ with a co-reactant depends on a great variety of parameters: nature of the co-reactant, electrode material, solvent, pH, presence of surfactant in the solution, respective concentrations of the co-reactant and of the ruthenium complex, hydrophobicity of the electrode surface, etc. [11]. By example, at high concentrations of $Ru(bpy)_3^{2+}$ (>0.1 mM), the "catalytic route" (also called EC′ route) is the dominant process for ECL [16–18]. Along this path, the catalytic oxidation of TPrA occurs by a reaction with electrogenerated $Ru(bpy)_3^{3+}$. Modified forms of the ruthenium complex are used to label biological molecules. These species keeps the ECL capabilities and undergoes an oxidative-reduction path in the presence of tri-*n*-propylamine. This technique is widely applied in immunoassays and nucleic acid assays [11].

ECL merges intimately electrochemical and optical aspects. The initiation of the phenomenon is an electrochemical step, whereas the analytical information is usually contained in the light signal. Combining both facets yields also important insights in the ECL mechanism. Accordingly, a variety of opto-electrochemical devices based on optical fibers has thus been developed. Ring microelectrodes were fabricated initially by coating a single optical fiber with gold or other electrically conductive materials [13,14,19–25]. Single optical fibers embedded into a "cage" or modified with a mini-grid have also been reported [15,26]. A new "electroptode" immuno-sensor have been developed to detect cholera antitoxin antibodies [27,28]. An ECL-based imaging fiber electrode chemical sensor has been applied for the detection of NADH [8]. An imaging fiber was coated with a gold layer and modified by a Nafion film. However, the transmission of the ECL light was relatively low through the gold layer. Random and ordered array of transparent electrodes have been applied for ECL measurements [29–32]. Using ECL imaging of the modified bundle's distal face, the ECL behavior of an electrode array and the diffusional decoupling between individual electrodes of the array has been studied [33]. Recently, we described the electrochemical properties and the far-field characterization of an array of nanoapertures with adjustable dimensions [34–36].

In this report, we present an array comprising thousands of nanoapertures for the ECL imaging of NADH concentration. Such a high-density array was fabricated on the distal face of a coherent optical fiber bundle. The fabrication steps of our approach produced an ordered array of nanoapertures, which retains the optical fiber bundle architecture. Therefore, the array keeps the imaging properties of the bundle at the micrometer scale. We also report the voltammetric and ECL signals of NADH with $Ru(bpy)_3^{2+}$ on a gold electrode. $Ru(bpy)_3^{2+}$ is used to mediate the NADH oxidation. Each nanoaperture is surrounded by a gold nanoring, which serves as an electrode material and also to confine light in each fiber core. The comparison of the nanoaperture array and of the macroelectrode shows similar electrochemical properties and ECL performances. Remote ECL imaging of NADH is achieved through the microarray of nanoapertures. ECL light is generated at the distal face of the array by each gold ring electrode. A fraction of this ECL light is collected by the corresponding nanoaperture, transmitted through the optical fiber bundle and finally imaged on the proximal face. In other words, ECL image is acquired through the nanoaperture array itself with a micrometer resolution.

2. Experimental

2.1. Materials

Ammonium fluoride (NH_4F, 99.99%), hydrofluoric acid (HF, 48 wt.% in water, 99.99%), acetic acid, NADH, phosphate-buffered saline (PBS, pH=7.5) and tris(2,2′-bipyridine) ruthenium(II) chloride ($Ru(bpy)_3Cl_2$) were obtained from Aldrich. The insulating varnish (Monoliss' Satin Blanc 01) was obtained from ICI Dulux Valentine. The cathodic electrophoretic paint (BASF FT83-0250) was a gift from BASF. Contacts were made with High Purity Silver paint (SPI,

West Chester, PA). The contact wires used were Kynar Insulated 30 awg wrapping wires (RS). All aqueous solutions were prepared with Milli-Q purified water (Millipore).

2.2. Apparatus and procedures

The potentiostat used was a PGSTAT 12 Autolab (Eco-Chemie). The working macroelectrode was a commercial gold electrode (Bioanalytical Systems, BAS). The quasi-reference and counter electrodes were Ag–AgCl and platinum wire respectively. The surface of the gold macroelectrode was polished with 30–15–3–0.3 μm lapping films (Thorlabs Inc.) and finally on a microcloth (Buehler) with a deagglomerated 0.05 μm alumina suspension (Buehler). SEM images were obtained with a scanning electron microscope (JOEL).

The instrument used for remote ECL imaging was a modified epifluorescence microscope (BX-30, Olympus). ECL light transmitted through the optical fiber bundle was collected by a 20× microscope objective, filtered by a band-pass filter (605±25 nm) and detected by a two-dimensional detector, such as a charge coupled device (CCD) camera. Therefore, ECL intensities of all the nanoapertures forming the array are captured simultaneously and individually at a given time in a single image. The ECL images were acquired by a charge coupled device (CCD) camera (Roper Scientific), which is fitted with a back-illuminated chip (Marconi 47-10) that has 1024 × 1024 pixels. The camera head cools the chip thermo-electrically to −40 °C and has a mechanical shutter. A computer controls the camera, collects and processes all the 16-bit coded images.

2.3. Fabrication of the nanoaperture array

Silica imaging fibers of 8 cm length with a total diameter of 350 μm comprising 6000 individually cladded 3–4 μm diameter optical fibers were purchased from Sumitomo Electric Industries (IGN-035/06). The active area and the numerical aperture (NA) of the coherent optical fiber bundle were 270 μm and 0.35, respectively. The distal face of the array was polished before use with 30–15–3–0.3 μm lapping films (Thorlabs). The polished side was then placed horizontal for 5 h into a buffered etching solution containing 500 μl of 40% (wt/wt) aqueous NH_4F solution, 100 μl of a 48% HF solution and 100 μl deionized water. (Caution: HF etching solutions are extremely corrosive!). The insulating jacket of the bundle was then removed with chloromethane and sonicated in water for 30 s to remove any residuals. The distal face of the resulting nanotip array was sputter-coated with a gold layer and connected to a copper wire with a high-purity conductive silver paint. Thus the electrode surface corresponds only to the gold-coated surface of the etched bundle. This gold-coated nanotip array was insulated using an electrophoretic paint. The distal face is immersed in a dilute aqueous paint solution with a volume fraction 1:1 of 3 mM acetic acid/cathodic electropho-

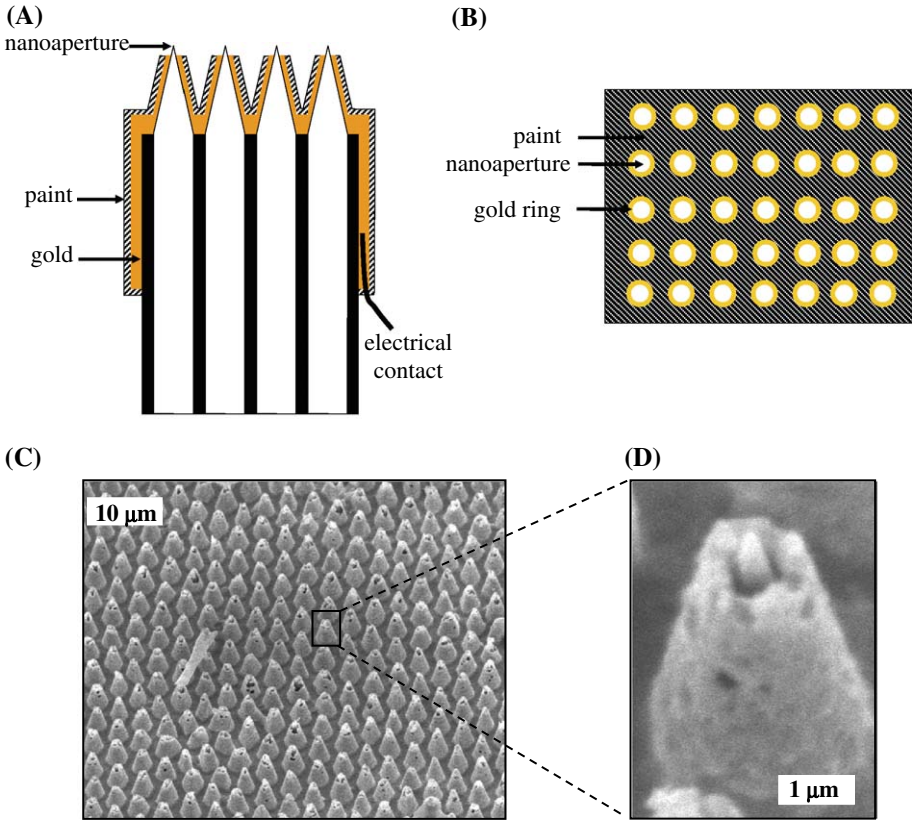

Fig. 1. Schematic illustration of the nanoaperture array (A: side view, B: top view). (C) Scanning electron micrograph of the distal face of the nanoaperture array. (D) High magnification allows viewing in details a nanoaperture of the array.

retic paint. The potential is scanned from 0 to −2.5 V/Ag–AgCl at 20 mV/s. The insulated array is cured at 180 °C for 1 h. While curing, the paint retracts from the tips exposing the gold electrode surface. The etching of the exposed gold layer at the tip apices is done with a classic KI/I_2 aqueous solution for 30 s.

3. Results and discussion

3.1. Fabrication and characterization

The fabrication steps of the nanoaperture array have been detailed elsewhere [29,34,35]. In brief, a coherent optical fiber bundle formed the base of our nanoaperture array. The coherent structure of the bundle used in this work transmits an image through the imaging fiber with a micrometric resolution [37]. A nanotip array is prepared by wet chemical etching of a coherent optical fiber bundle comprising 6000 individually cladded 3–4 μm diameter optical fibers. Conical nanotips were created at each optical fiber core by using the difference in etching rates between the GeO_2-doped core and the fluorine-doped clad [38–40]. The surface of the nanotip array was then sputter-coated with a gold film and the entire array surface was insulated with an electrophoretic paint except for the tip apex. In order to create the optical nanoapertures, the exposed gold film is removed by reacting in a gold-etching solution. So we produced an ordered array where each optical nanoaperture is surrounded by a gold ring-shaped electrode (Fig. 1). Since the electromagnetic field decays exponentially inside the metal, the gold film serves to confine light to the tip apex as in aperture SNOM. In addition, the gold nanoring is also used as the electrode material to perform electrochemical reactions. Fig. 1C shows the scanning electron micrograph of the array surface. The ordered structure of the nanoapertures and the homogeneity of the array are clearly visible. At high magnification (Fig. 1D), one can observe the central aperture corresponding to the etched core, which is surrounded successively by a gold film and eventually an insulating paint layer.

To thoroughly characterize the array, we imaged the surface of the distal face by atomic force microscopy with a conductive probe [41,42]. This scanning probe technique which works in contact mode provides simultaneously the topography of the sample surface and the cartography of its local resistance with nanometer scale resolution (Fig. 2). Fig. 2A displays the topography of the samples. The resistance cartography (Fig. 2B) reveals that the resistance of the surface decreases at the nanotip apex. Indeed, the only conductive surface of the array is the gold nanorings surrounding the nanoapertures. No pinholes were observed on the surface. Fig. 2C displays a single nanoaperture at high magnification. The yellow zone corresponds to area with high resistance, in other words; to the paint insulating region. The dark triangle corresponds to a region with high conductivity, which represents the gold ring film. This figure shows directly the image of the gold nanoring. However, since the size of our nanoapertures is similar to those of the AFM probe, the convolution of the AFM tip with the array surface distorts the collected images (Fig. 2). The "arrow" shape of our aperture observed on Fig. 2C is related to the scanning direction and reflects the convolution by the scanning AFM tip. Indeed, when we changed the scanning direction, we modified the orientation of this "arrow". However, one can observe that the structure of the gold ring is regular.

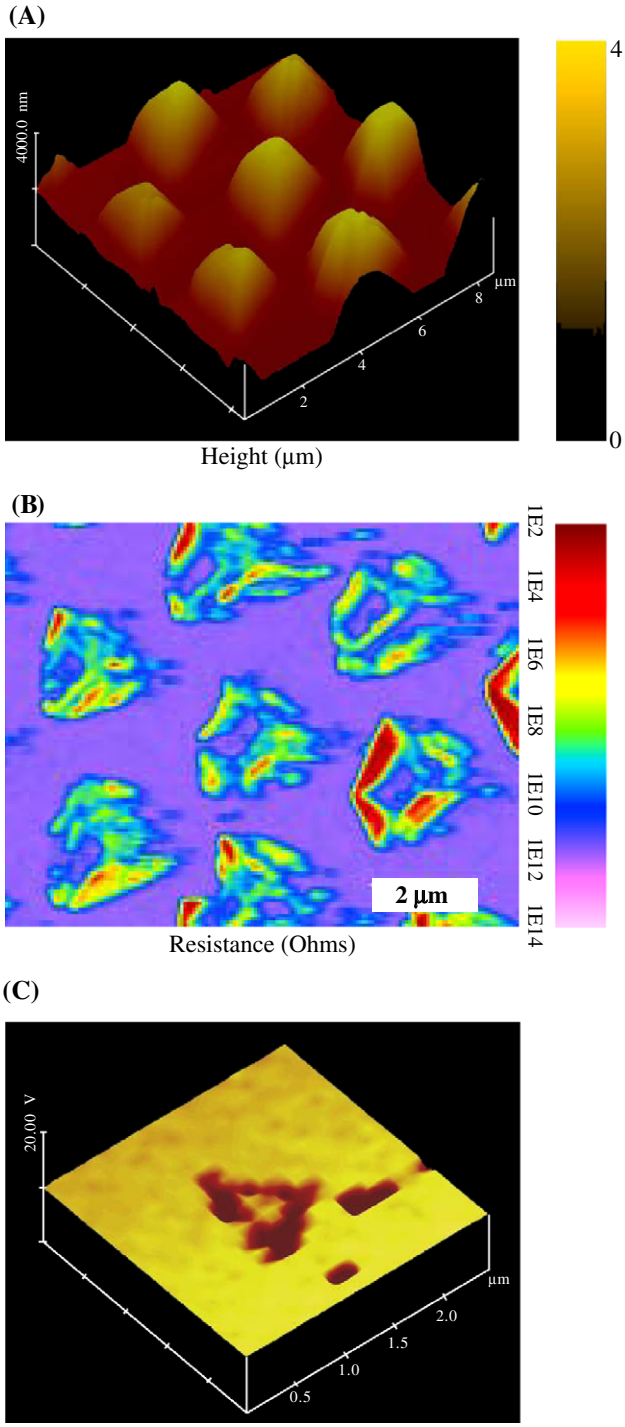

Fig. 2. (A) Topographic and (B) resistance images of the nanoaperture array obtained by AFM with a conductive tip. (C) Resistance image at high magnification of the gold nanoring surrounding the optical nanoaperture.

3.2. Electrochemical and ECL properties

The main goal of this work is to study the electrochemical and the ECL properties of the array of nanoapertures surrounded by the gold nanorings. We compare the behavior of the array with those of a gold bare macroelectrode. We present also some preliminary results about the ECL process of NADH with $Ru(bpy)_3^{2+}$. The ECL mechanisms of $Ru(bpy)_3^{2+}$ with oxalate and tri-*n*-propylamine have been investigated by various groups [16–18,43–48]. But, to our knowledge, similar electrochemical studies of the ECL mechanism have not been performed with NADH. Recently, mechanism of electron transfer oxidation of NADH and of analogues has been reported [49]. The chemiluminescence process of NADH analogues with $Ru(bpy)_3^{3+}$ has been also presented [49]. However, no electrochemical data were presented in this work.

Cyclic voltammetry was utilized to characterize the electrochemical properties. Fig. 3A displays the voltammogram of a bare gold macroelectrode immersed in a PBS solution containing the ruthenium complex (solid line). It shows a classical transient response for this well-known reversible couple. The array shows a similar response for the $Ru(bpy)_3^{2+}$ solution. The oxidation and reduction peaks occur at the same potentials for both electrodes. It indicates that the gold nanoring array has excellent electrochemical performance. On the gold macroelectrode, NADH is irreversibly oxidizes at 0.8 V/Ag–AgCl. The oxidation of NADH is chemically irreversible due to rapid protonation kinetics occurring in the $NAD^+/NAD^\bullet$ redox couple [8]. At $E=0$ V/Ag–AgCl, no electrode reaction occurs and there was no detectable ECL light (Fig. 3A, squares). When the potential of the macroelectrode moves to potentials where NADH oxidation takes place, ECL is still not initiated. In fact, ECL intensity increased rapidly and reached almost a plateau value only at the potential matching the $Ru(bpy)_3^{2+}$ oxidation wave. In addition, the ECL spectrum corresponds to the emission of the $Ru(bpy)_3^{2+}$ species (data not shown). It is

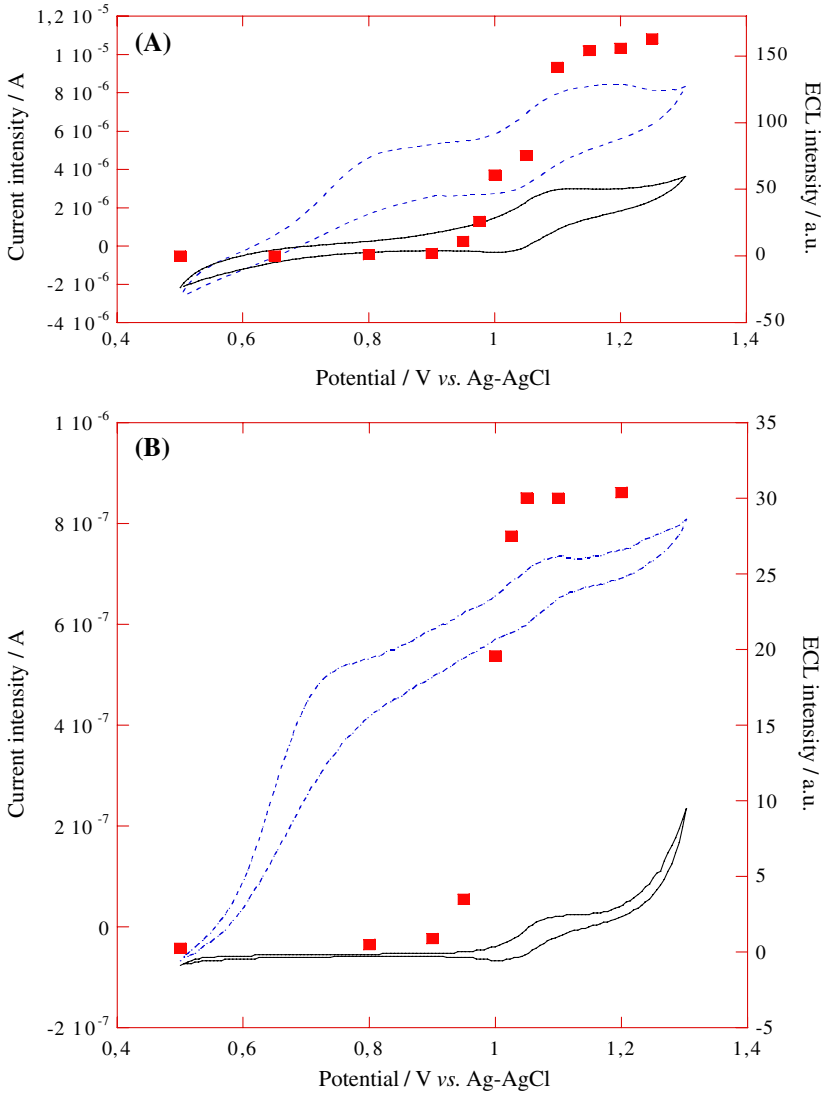

Fig. 3. Influence of the potential on the ECL intensity (squares) and on the faradaic current measured in absence (solid line) and in presence (dashed line) of NADH with (A) a gold macroelectrode or (B) through the nanoaperture array. Solutions were (A) 1 mM $Ru(bpy)_3^{2+}$/5 mM NADH and (B) 1 mM $Ru(bpy)_3^{2+}$/10 mM NADH in PBS buffer (pH=7.5). $v=50$ mV s^{-1}.

the typical MLCT emission (λ_{max}=610 nm) of the $Ru(bpy)_3^{2+*}$ in water at room temperature [50].

Fig. 3B summarizes the electrochemical and ECL responses of the array as a function of the applied potential. The NADH oxidation wave is irreversible and located at 0.8 V/Ag–AgCl. The wave intensity is higher than in Fig. 3A since the NADH concentration has been increased twofold. This figure shows the effect of the potential on the ECL intensity acquired through the array itself (squares) and on the faradaic current (dashed line). We want to emphasize that the ECL intensity is detected through the nanoaperture array. No ECL light is generated before the oxidation wave of $Ru(bpy)_3^{2+}$. So the gold macroelectrode and the gold nanoring array display similar characteristics for the electrochemistry of NADH and of the ruthenium complex. In the same way, the ECL behavior is identical. This study demonstrates that the gold nanorings behave as bare gold even if it was sputtered-coated on the optical fiber bundle and then chemically etched to form the nanoapertures.

On gold, the cyclic voltammogram of a PBS solution containing both NADH and $Ru(bpy)_3^{2+}$ shows well-separated waves (Fig. 3). No ECL emission is observed at potentials where only oxidation of NADH occurs. In fact, ECL is initiated only at potentials sufficiently positive to cause $Ru(bpy)_3^{2+}$ oxidation. The mechanism of this ECL reaction clearly involves reaction of $Ru(bpy)_3^{3+}$ and an intermediate species formed on oxidation of NADH. A recent study indicates that an homogeneous electron transfer from a neutral radical of a NADH analogue and $Ru(bpy)_3^{3+}$ occurs to produce the excited state, $Ru(bpy)_3^{2+*}$ [49]. The ECL process can be described by the following reaction scheme where an oxidative-reductive sequence occurs:

$$NADH \rightarrow NADH^{\bullet +} + e^- \quad (1)$$

$$Ru(bpy)_3^{2+} \rightarrow Ru(bpy)_3^{3+} + e^- \quad (2)$$

$$Ru(bpy)_3^{3+} + NADH \rightarrow Ru(bpy)_3^{2+} + NADH^{\bullet +} \quad (3)$$

$$NADH^{\bullet +} \rightarrow NAD^{\bullet} + H^+ \quad (4)$$

$$Ru(bpy)_3^{3+} + NAD^{\bullet} \rightarrow Ru(bpy)_3^{2+*} + NAD^+ \quad (5)$$

$$Ru(bpy)_3^{2+*} \rightarrow Ru(bpy)_3^{2+} + h\nu_{ECL}. \quad (6)$$

NADH and $Ru(bpy)_3^{2+}$ are oxidized at the electrode surface at their respective potentials. NADH can also be oxidized homogeneously by $Ru(bpy)_3^{3+}$. Then the radical cation $NADH^{\bullet +}$ deprotonates to form a highly reducing species (reaction 4). The reaction with $Ru(bpy)_3^{3+}$ leads to the excited state. This homogeneous electron transfer (reaction 5) is exergonic enough to populate the excited state of the ruthenium complex (2.12 eV) [51]. The initial electron transfer from NADH to $Ru(bpy)_3^{3+}$ is not exergonic enough to generate the excited state [49]. Eventually, $Ru(bpy)_3^{2+*}$ returns to the ground state by emitting a photon (λ_{max}=610 nm). Further studies focused on this issue are required to definitely establish the ECL mechanism.

3.3. Remote ECL imaging of NADH

The device presented in this work integrates several functions in an array format. Indeed, the nanoaperture array serves to concomitantly initiate, transmit and detect the ECL emission through the imaging fiber bundle itself. On Fig. 4, the distal face of the bundle is immersed in a PBS solution containing both $Ru(bpy)_3^{2+}$ and NADH. When a suitable anodic potential is applied to the array, each gold nanoring electrode oxidizes $Ru(bpy)_3^{2+}$ and thus initiates locally the ECL emission. In other words, discrete ECL microspots are electrogenerated by the gold nanorings forming the array (Fig. 4). ECL light generated by the gold nanoring electrode and collected by the corresponding nanoaperture propagates under guided conditions in the fiber core by total internal reflection (Fig. 4). In fact, the core diameter varies slightly to minimize cross-talk between the cores and to improve spatial resolution when used as imaging fibers [52]. ECL emission was filtered by a band-pass filter (605±25 nm) to ensure that only ECL wavelength was detected. Finally, a microscope fitted with a CCD camera collects the ECL image of the proximal face of the entire optical fiber bundle. It means that, with a single image, we can remotely measure the ECL intensity generated by all the nanorings, collected by all the nanoapertures and eventually transmitted by all the cores. Therefore, the nanoapertures are individually readable with a CCD camera. Fig. 5 displays the false color image of a representative region of interest of the nanoaperture array when ECL is generated. One can see the cores, which transmit ECL light surrounded by the clad. This image shows the proximal face of about 2500 individual

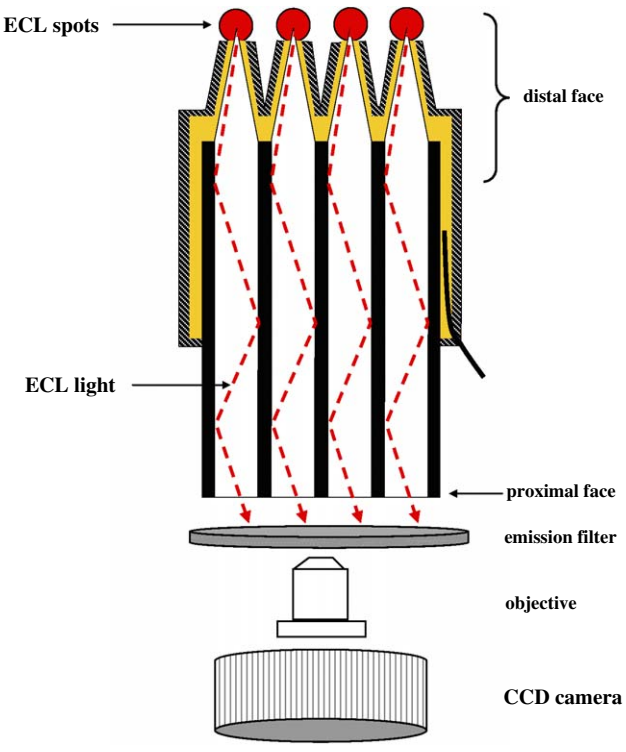

Fig. 4. Schematic representation showing the experimental layout.

optical fibers, which correspond to 2500 nanoapertures. In brief, a single image acquired with the CCD camera allows to measure simultaneously and individually the ECL intensities of all the nanoapertures forming the array.

A fraction of the isotropically generated ECL by a nanoring electrode is collected by the same nanoaperture whereas neighboring nanoapertures could also collect it. This latter fraction is function of the acceptance cone of the apertures, on the size of the ECL-emitting layer, on the geometry of the array, on the distance between adjacent tips and on a term proportional to the square of the distance, which is related to the isotropically expanding sphere of emitted ECL. The contribution of the ECL is highly dependent on the distance and decreases extremely fast with it. Thus, the ECL signal originates essentially from the volume located very close to the nanoaperture. This result can be also explained by taking into account the effective cross section of a nanoaperture. We consider the ECL intensity that is generated at a nanoaperture and that falls onto an adjacent one. Since the radius of the aperture is ~200 nm (Fig. 1D), we assumed in a first approximation that each nanoaperture initiates an ECL point source at the tip apex. It is a reasonable approximation since the electrocatalytic mechanism confines the ECL layer to the electrode surface. From the SEM image (Fig. 1), the base radius and the height of the nanoapertures were estimated. Therefore, one can calculate the cross-section of a nanoaperture. Since the distance between adjacent tips is ~4 μm, the fraction of ECL emitted at one nanoaperture and collected by an adjacent one is less than 1%. This value is calculated just by considering the effective cross section. Furthermore, if we take into account also the acceptance cone of the nanoaperture, only a small part of ECL light generated at neighboring nanoapertures can be effectively collected and transmitted by the core. Indeed, in previous works, we reported the angular profile of the intensity transmitted by arrays of apertures with adjustable subwavelength dimensions, in the far-field regime [34,36]. Therefore, the value of the former fraction can be considered as negligible. In conclusion, a nanoaperture collects only the ECL light generated by its nanoring and the nanoapertures forming the array are optically independent.

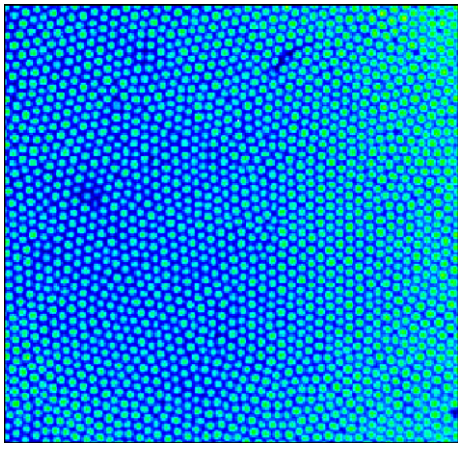

Fig. 5. ECL image of the proximal face of the array acquired after the application of 1.2 V. Solution was 1 mM $Ru(bpy)_3^{2+}$ and 10 mM NADH in PBS buffer (pH=7.5). The image is represented using a false color coding according to the color bar. Black represents low ECL light intensity.

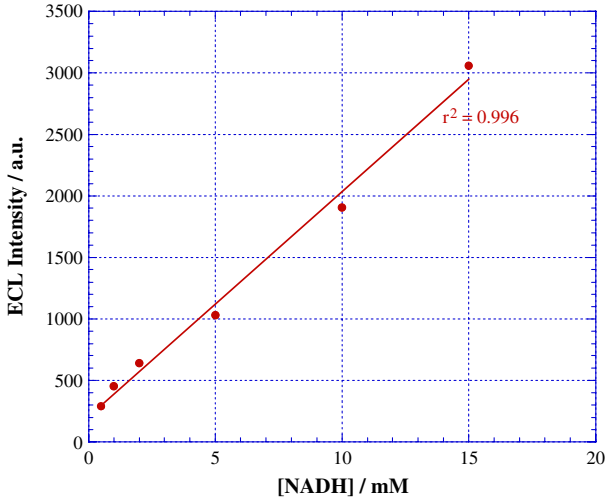

Fig. 6. Plot of ECL intensity vs. NADH concentration in solutions containing 1 mM $Ru(bpy)_3^{2+}$ in PBS buffer (pH=7.5). ECL calibration curve was obtained through the nanoaperture array.

3.4. Quantitative ECL imaging of NADH

At lower NADH concentrations, ECL intensity detected by the CCD camera is decreased (image not shown). A calibration curve was constructed to test the quantitative validity of this remote imaging approach. When the potential was held constant at E=1.2 V/Ag–AgCl, the ECL signal was constant for several minutes. We selected this potential to test the analytical performance of our nanoaperture array. Furthermore, the monitored ECL intensity was reproducible. ECL intensity was measured when the array was exposed to different NADH concentrations (Fig. 6). Plot of ECL intensity against the concentration of NADH was linear in the concentration range 0.5 mM to 15 mM. The line that passes through the data points in Fig. 6 is the linear regression fit. The correlation coefficient was 0.996. It shows that the ECL intensity is proportional to the NADH concentration. Furthermore, stable and reproducible ECL intensity responses are obtained allowing more than 30 reproducible assays.

4. Conclusions

In this work, we demonstrated that the presented nanoaperture array can be applied to the ECL detection of NADH. The fabrication steps produced an ordered array of nanoapertures, which retains the optical fiber bundle architecture. Therefore, the array keeps the imaging properties of the bundle at the micrometer scale. $Ru(bpy)_3^{2+}$ is used to mediate the NADH oxidation. This redox process leads to the formation of $Ru(bpy)_3^{2+*}$ and to the corresponding ECL emission. In fact, in this approach, NAD^+ is regenerated and an ECL signal is concomitantly emitted. Preliminary results on the ECL oxidative-reductive mechanism of NADH with $Ru(bpy)_3^{2+}$ are also reported on a gold electrode surface. Remote ECL imaging

of NADH is achieved through the microarray of nanoapertures. Indeed, ECL light is generated at the distal face of the array by each gold ring electrode. A fraction of this ECL light is then collected by the corresponding nanoaperture, transmitted through the optical fiber bundle and finally imaged on the proximal face. Direct imaging of NADH concentrations has been performed quantitatively through the array itself. The ECL array also showed good temporal stability and reproducibility. In future work, we plan to couple a dehydrogenase enzyme that converts NAD^+ to NADH with the sensor array in order to develop an imaging ECL biosensor array. The ECL light would then be enzymatically amplified and this step should improve the sensitivity and the detection limit.

Acknowledgments

The authors thank Gilles Pecastaings and Hassan Saadaoui (Centre de Recherche Paul Pascal-CNRS, Université Bordeaux I) for the AFM pictures and Gilles Lovo (BASF) for the gift of the electrophoretic paint.

References

[1] P.N. Bartlett, E. Simon, C.S. Toh, Modified electrodes for NADH oxidation and dehydrogenase-based biosensors, Bioelectrochemistry 56 (2002) 117–122.
[2] F.D. Munteanu, N. Mano, A. Kuhn, L. Gorton, Mediator-modified electrodes for catalytic NADH oxidation: high rate constants at interesting overpotentials, Bioelectrochemistry 56 (2002) 67–72.
[3] L.L. Shultz, J.S. Stoyanoff, T.A. Nieman, Temporal and spatial analysis of electrogenerated $Ru(bpy)_3^{2+}$ chemiluminescent reactions in flowing streams, Anal. Chem. 68 (1996) 349–354.
[4] W.-Y. Lee, T.A. Nieman, Evaluation of use of tris(2,2′-bipyridyl)ruthenium(III) as a chemiluminescent reagent for quantitation in flowing stream, Anal. Chem. 67 (1995) 1789–1796.
[5] A.F. Martin, T.A. Nieman, Chemiluminescence biosensors using tris(2,2′-bipyridyl)ruthenium(II) and dehydrogenases immobilized in cation exchange polymers, Biosens. Bioelectron. 12 (1997) 479–489.
[6] T.M. Downey, T.A. Nieman, Chemiluminescence detection using regenerable tris(2,2′-bipyridyl)ruthenium(II) immobilized in Nafion, Anal. Chem. 64 (1992) 261–268.
[7] F. Jameison, R.I. Sanchez, L. Dong, J.K. Leland, D. Yost, M.T. Martin, Electrochemiluminescence-based quantitation of classical clinical chemistry analytes, Anal. Chem. 68 (1996) 1298–1302.
[8] E.S. Jin, B.J. Norris, P. Pantano, An electrogenerated chemiluminescence imaging fiber electrode chemical sensor for NADH, Electroanalysis 13 (2001) 1287–1290.
[9] A.F. Martin, T.A. Nieman, Glucose quantitation using an immobilized glucose dehydrogenase enzyme reactor and a tris(2,2′-bipyridyl)ruthenium(II) chemiluminescent sensor, Anal. Chim. Acta 281 (1993) 475–481.
[10] L.R. Faulkner, A.J. Bard, Techniques of electrogenerated chemiluminescence, in: A.J. Bard (Ed.), Electroanalytical Chemistry, M. Dekker, New-York, 1977, pp. 1–95.
[11] M.M. Richter, Electrochemiluminescence (ECL), Chem. Rev. 104 (2004) 3003–3036.
[12] M.-L. Calvo-Muñoz, A. Dupont-Filliard, M. Billon, S. Guillerez, G. Bidan, C. Marquette, L. Blum, Detection of DNA hybridization by ABEI electrochemiluminescence in DNA-chip compatible assembly, Bioelectrochemistry 66 (2005) 139–143.
[13] L.S. Kuhn, A. Weber, S.G. Weber, Microring electrode/optical waveguide: electrochemical characterization and application to electrogenerated chemiluminescence, Anal. Chem. 62 (1990) 1631–1636.
[14] C.B. Cohen, S.G. Weber, Photoelectrochemical sensor for catalase activity based on the in situ generation and detection of substrate, Anal. Chem. 65 (1993) 169–175.
[15] H. Wang, G. Xu, S. Dong, Electrochemiluminescent microoptoprobe with mini-grid working electrode and self-contained sample container, Electrochem. Commun. 4 (2002) 214–217.
[16] Y. Zu, A.J. Bard, Electrogenerated chemiluminescence: 66. The role of direct coreactant oxidation in the ruthenium tris(2,2′)bipyridyl/tripropylamine system and the effect of halide ions on the emission intensity, Anal. Chem. 72 (2000) 3223–3232.
[17] F. Kanoufi, Y. Zu, A.J. Bard, Homogeneous oxidation of trialkylamines by metal complexes and its impact on electrogenerated chemiluminescence in the trialkylamine/$Ru(bpy)_3^{2+}$ system, J. Phys. Chem., B 105 (2001) 210–216.
[18] E.M. Gross, P. Pastore, R.M. Wightman, High-frequency electrochemiluminescent investigation of the reaction pathway between tris(2,2′-bipyridyl)ruthenium(II) and tripropylamine using carbon fiber microelectrodes, J. Phys. Chem., B 105 (2001) 8732–8738.
[19] G.I. Pennarun, C. Boxall, D. O'Hare, Micro-optical ring electrode: development of a novel electrode for photoelectrochemistry, Analyst 121 (1996) 1779–1788.
[20] D.A. Van Dyke, H.Y. Cheng, Fabrication and characterization of a fiber-optic-based spectroelectrochemical probe, Anal. Chem. 60 (1988) 1256–1260.
[21] P.J.S. Smith, P.G. Haydon, A. Hengstenberg, S.-K. Jung, Analysis of cellular boundary layers: application of electrochemical microsensors, Electrochim. Acta 47 (2001) 283–292.
[22] N. Casillas, P. James, W.H. Smyrl, A novel approach to combine scanning electrochemical microscopy and scanning photoelectrochemical microscopy, J. Electrochem. Soc. 142 (1995) L16–L18.
[23] Y. Lee, S. Amemiya, A.J. Bard, Scanning electrochemical microscopy: 41. Theory and characterization of ring electrodes, Anal. Chem. 73 (2001) 2261–2267.
[24] Y. Lee, A.J. Bard, Fabrication and characterization of probes for combined scanning electrochemical/optical microscopy experiments, Anal. Chem. 74 (2002) 3626–3633.
[25] Y. Lee, Z. Ding, A.J. Bard, Combined scanning electrochemical/optical microscopy with shear force and current feedback, Anal. Chem. 74 (2002) 3634–3643.
[26] D.A. VanDyke, H.Y. Cheng, Electrochemical manipulation of fluorescence and chemiluminescence signals at fiber-optic probes, Anal. Chem. 61 (1989) 633–636.
[27] R.S. Marks, A. Novoa, T. Konry, R. Krais, S. Cosnier, Indium tin oxide-coated optical fiber tips for affinity electropolymerization, Mater. Sci. Eng., C, Biomim. Mater., Sens. Syst. 21 (2002) 189–194.
[28] T. Konry, A. Novoa, S. Cosnier, R.S. Marks, Development of an "Electroptode" immunosensor: indium tin oxide-coated optical fiber tips conjugated with an electropolymerized thin film with conjugated cholera toxin B subunit, Anal. Chem. 75 (2003) 2633–2639.
[29] S. Szunerits, P. Garrigue, J.-L. Bruneel, L. Servant, N. Sojic, Fabrication of a sub-micrometer electrode array: electrochemical characterization and mapping of an electroactive species by confocal raman microspectroscopy, Electroanalysis 15 (2003) 548–555.
[30] A. Chovin, P. Garrigue, P. Vinatier, N. Sojic, Development of an ordered array of optoelectrochemical individually readable sensors with submicrometer dimensions: application to remote electrochemiluminescence imaging, Anal. Chem. 76 (2004) 357–364.
[31] S. Szunerits, D.R. Walt, Fabrication of an optoelectrochemical microring array, Anal. Chem. 74 (2002) 1718–1723.
[32] A. Chovin, P. Garrigue, N. Sojic, Electrochemiluminescent detection of hydrogen peroxide with an imaging sensor array, Electrochim. Acta 49 (2004) 3751–3757.
[33] S. Szunerits, J.M. Tam, L. Thouin, C. Amatore, D.R. Walt, Spatially resolved electrochemiluminescence on an array of electrode tips, Anal. Chem. 75 (2003) 4382–4388.
[34] A. Chovin, P. Garrigue, I. Manek-Hönninger, N. Sojic, Fabrication, characterization and far-field optical properties of an ordered array of nanoapertures, Nano Lett. 4 (2004) 1965–1968.

[35] A. Chovin, P. Garrigue, L. Servant, N. Sojic, Electrochemical modulation of remote fluorescence imaging at an ordered opto-electrochemical nanoaperture array, ChemPhysChem 5 (2004) 1125–1132.
[36] A. Chovin, P. Garrigue, G. Pecastaings, H. Saadaoui, I. Manek-Hönninger, N. Sojic, Microarrays of near-field optical probes with adjustable dimensions. Ultramicroscopy (in press).
[37] P. Pantano, D.R. Walt, Analytical applications of optical imaging fibers, Anal. Chem. 67 (1995) 481A–487A.
[38] M. Ohstu, Photon STM: from imaging to fabrication, Optoelectronics 10 (1995) 147–166.
[39] P. Pantano, D.R. Walt, Toward a near-field optical array, Rev. Sci. Instrum. 68 (1997) 1357–1359.
[40] Y.-H. Liu, T.H. Dam, P. Pantano, A pH-sensitive nanotip array imaging sensor, Anal. Chim. Acta 419 (2000) 215–225.
[41] F. Houzé, R. Meyer, O. Schneegans, L. Boyer, Imaging the local electrical properties of metal surfaces by atomic force microscopy with conducting probes, Appl. Phys. Lett. 69 (1996) 1975–1977.
[42] J. Ravier, F. Houze, F. Carmona, O. Schneegans, H. Saadaoui, Mesostructure of polymer/carbon black composites observed by conductive probe atomic force microscopy, Carbon 39 (2001) 314–318.
[43] F. Kanoufi, A.J. Bard, Electrogenerated chemiluminescence: 65. An investigation of the oxidation of oxalate by tris(polypyridine) ruthenium complexes and the effect of the electrochemical steps on the emission intensity, J. Phys. Chem., B 103 (1999) 10469–10480.
[44] F. Kanoufi, C. Cannes, Y. Zu, A.J. Bard, Scanning electrochemical microscopy: 43. Investigation of oxalate oxidation and electrogenerated chemiluminescence across the liquid–liquid interface, J. Phys. Chem., B 105 (2001) 8951–8962.
[45] R.Y. Lai, A.J. Bard, Electrogenerated chemiluminescence: 70. The application of ECL To determine electrode potentials of tri-*n*-propylamine, its radical cation, and intermediate free radical in MeCN/benzene solutions, J. Phys. Chem., A 107 (2003) 3335–3340.
[46] Y. Zu, A.J. Bard, Electrogenerated chemiluminescence: 67. Dependence of light emission of the Tris(2,2¢)bipyridylruthenium(II)/tripropylamine system on electrode surface hydrophobicity, Anal. Chem. 73 (2001) 3960–3964.
[47] W. Miao, J.-P. Choi, A.J. Bard, Electrogenerated chemiluminescence: 69. The Tris(2,2¢-bipyridine)ruthenium(II), $(Ru(bpy)_3^{2+})$/tri-*n*-propylamine (TPrA) system revisited. A new route involving TPrA•+ cation radicals, J. Am. Chem. Soc. 124 (2002) 14478–14485.
[48] M. Zhou, J. Heinze, K. Borgwarth, C.P. Grover, Direct voltammetric evidence for a reducing agent generated from the electrochemical oxidation of tripropylamine for electrochemiluminescence of ruthenium tris(bipyridine) complexes? ChemPhysChem 4 (2003) 1241–1243.
[49] S. Fukuzumi, O. Inada, T. Suenobu, Mechanisms of electron-transfer oxidation of NADH analogues and chemiluminescence. Detection of the keto and enol radical cations, J. Am. Chem. Soc. 125 (2003) 4808–4816.
[50] K. Kalyansundaram, Photophysics, photochemistry and solar energy conversion with tris(bipyridyl)ruthenium(II) and its analogues, Coord. Chem. Rev. 46 (1982) 159–244.
[51] W.L. Wallace, A.J. Bard, Electrogenerated chemiluminescence: 35. Temperature dependence of the ECL efficiency of $Ru(bpy)_3^{2+}$ in acetonitrile and evidence for very high excited state yields from electron transfer reactions, J. Phys. Chem. 83 (1979) 1350–1357.
[52] M. Mogi, K. Yoshimura, Development of super high density packed image guide, Proc. SPIE Int. Soc. Opt. Eng. 1067 (1989) 172–181.